JACS
JOURNAL OF THE AMERICAN CHEMICAL SOCIETY
pubs.acs.org/JACS

Article

Catalytic Reduction of Cyanide to Ammonia and Methane at a Mononuclear Fe Site

Christian M. Johansen and Jonas C. Peters*

Cite This: J. Am. Chem. Soc. 2024, 146, 5343−5354

Read Online

ACCESS | Metrics & More | Article Recommendations | Supporting Information

ABSTRACT: Nitrogenase enzymes catalyze nitrogen reduction (N_2R) to ammonia and also the reduction of non-native substrates, including the $7H^+/6e^-$ reduction of cyanide to CH_4 and NH_3. CN^- and N_2 are isoelectronic, and it is hence fascinating to compare the mechanisms of synthetic Fe catalysts capable of both CN^- and N_2 reduction. Here, we describe the catalytic reduction of CN^- to NH_3 and CH_4 by a highly selective $(P_3^{Si})Fe(CN)$ catalyst (P_3^{Si} represents a tris(phosphine)silyl ligand). Catalysis is driven in the presence of excess acid ($[Ph_2NH_2]OTf$) and reductant ($(C_6H_6)_2Cr$), with turnover as high as 73 demonstrated. This catalyst system is also modestly competent for N_2R and structurally related to other tris(phosphine)Fe-based N_2R catalysts. The choice of catalyst and reductant is important to observe high yields. Mechanistic studies elucidate several intermediates of CN^- reduction, including iron isocyanides ($P_3^{Si}FeCNH^{+/0}$) and terminal iron aminocarbynes ($P_3^{Si}FeCNH_2^{+/0}$). Aminocarbynes are isoelectronic to iron hydrazidos ($Fe{=}N{-}NH_2^{+/0}$), which have been invoked as selectivity-determining intermediates of N_2R (NH_3 versus N_2H_4 products). For the present CN^- reduction catalysis, reduction of aminocarbyne $P_3^{Si}FeCNH_2^+$ is proposed to be rate but not selectivity contributing. Instead, by comparison with the reactivity of a methylated aminocarbyne analogue ($P_3^{Si}FeCNMe_2$), and associated computational studies, formation of a Fischer carbene ($P_3^{Si}FeC(H)(NH_2)^+$) intermediate that is on path for either CH_4 and NH_3 (6 e^-) or CH_3NH_2 (4 e^-) products is proposed. From this carbene intermediate, pathways to the observed CH_4 and NH_3 products (distinct from CH_3NH_2 formation) are considered to compare and contrast the (likely) mechanism/s of CN^- and N_2 reduction.

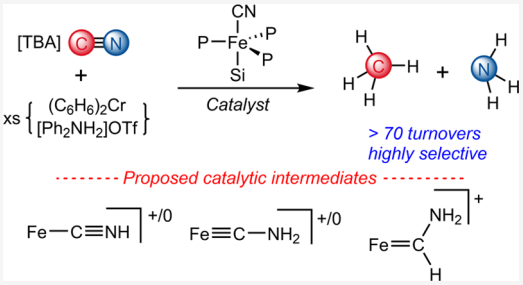

INTRODUCTION

Nitrogenases catalyze nitrogen reduction to ammonia (N_2R) as well as the reductive protonation of non-native substrates,[1−4] including cyanide (CN^-).[5−13] These are mechanistically fascinating bioorganometallic transformations which, for the case of CN^- (and CO/CO_2 as well), may involve metal-to-carbon intermediates such as alkyls, carbenes, and carbynes/carbides that are conceptually related to posited intermediates of N_2R (e.g., NNH, NNH_2, NH).

Whereas substantial attention from the synthetic community has been directed toward functional N_2R models with associated mechanistic studies,[14−16] there has been only limited attention paid to catalytic cyanide reduction by comparison.[17−22] Given potential mechanistic parallels between catalytic N_2 and CN^- reduction, including an isolobal relationship between aminocarbynes (e.g., $M{\equiv}CNR_2$)[23−26] and their hydrazido ($M{=}NNR_2$) counterparts,[27−29] mechanistically well-defined CN^- reduction catalysts present an attractive target for further study. In contrast to terminal hydrazido systems, the reductive protonation of terminal carbynes to liberate products (e.g., CH_4/NH_3) has rarely been observed.[25,30−33] Indeed, catalytic transformations involving *bona fide* carbyne intermediates, outside of the scope of metathesis reactions,[34,35] are essentially without precedent.

Toward these objectives, our lab reported in 2016 a single-site iron model system capable of mediating the (sub)-stoichiometric reductive protonation of CN^- to CH_4 and NH_3.[25] We also characterized a number of species as plausible intermediates of the overall transformation, most notably the carbyne complex $(P_3^{Si})Fe(CNH_2)^+$ (P_3^{Si} represents a tris(phosphino)silyl ligand; Figure 1, top).[25] The product distribution observed mimics that of ATP-dependent cyanide reduction by nitrogenases (Figure 1, middle), where the major observed products under most conditions studied are methane and ammonia (6 e^- reduction); methylamine (H_3CNH_2; 4 e^- reduction) and methylenimine ($H_2C{=}NH$; 2 e^- reduction) can also be observed as minor products, along with trace ethane and ethylene.[6−9]

Several synthetic Fe−S clusters have also been shown to catalyze cyanide reduction and exhibit substantially higher selectivities for C−C coupled products than has been observed

Received: November 7, 2023
Revised: January 25, 2024
Accepted: January 26, 2024
Published: February 16, 2024

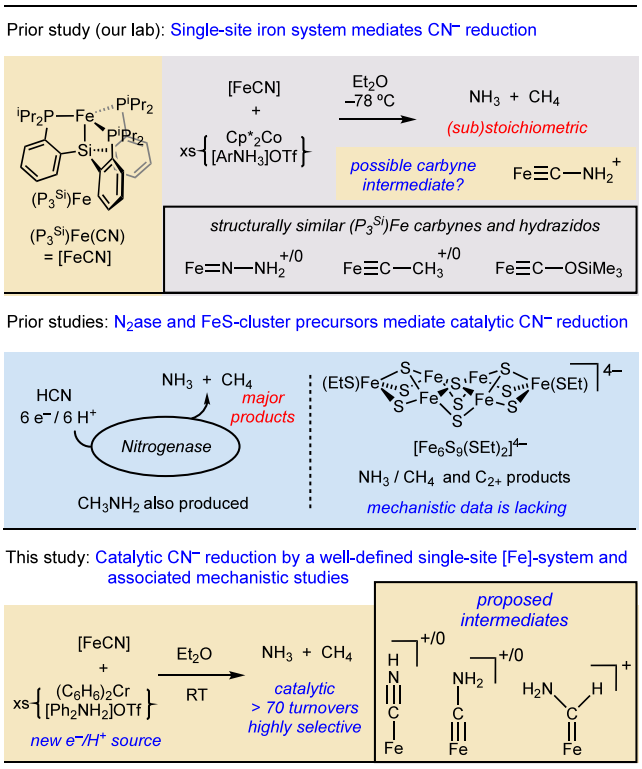

Figure 1. Summary of prior studies on stoichiometric and catalytic cyanide reductions mediated by iron complexes as a context for this study.

with nitrogenase enzymes as the catalysts (Figure 1, middle).[10−12,20−22] Catalytically relevant species in transformations employing such clusters as precatalysts are ill-defined, and to date, associated mechanistic information has not been forthcoming.

Against this backdrop, we have sought conditions for *catalytic* cyanide reduction via our well-defined (P_3^{Si})Fe system, ideally manifesting product distributions akin to nitrogenases (chiefly favoring the C_1 products CH_4 and CH_3NH_2) and amenable to mechanistic scrutiny. This study presents our findings (Figure 1, bottom).

Guided by measured and estimated thermochemical parameters (Figure 2a),[36] we show herein that the iron complex (P_3^{Si})Fe(CN) (abbreviated as [FeCN]) efficiently catalyzes cyanide reduction in the presence of acids and reductants. By employing a combination of synthetic, ^{57}Fe Mössbauer, optical, and theoretical studies, we outline a mechanistic scheme for the catalytic cycle, which can be juxtaposed with that of catalytic nitrogen fixation mediated by analogous iron complexes.

RESULTS

Canvassing Conditions for More Efficient [FeCN] Reduction. To target the catalytic reduction of CN^-, we sought conditions for the proton-coupled reduction of [FeCN] to produce NH_3/CH_4 (or CH_3NH_2) and an [Fe] byproduct that might re-enter a catalytic cycle. In our original report,[25] we described the proton-coupled reduction of [FeCN] using excess $[^{2,5\text{-Cl}}PhNH_3]OTf$ and Cp^*_2Co (pK_a 4.5 for $[^{2,5\text{-Cl}}PhNH_3]OTf$ in THF; all pK_a's reported in THF;[36] $E°$ = −1.9 V for Cp^*_2Co; all redox potentials are reported in THF and referenced to $Fc^{+/0}$).[37] Such reaction mixtures invariably

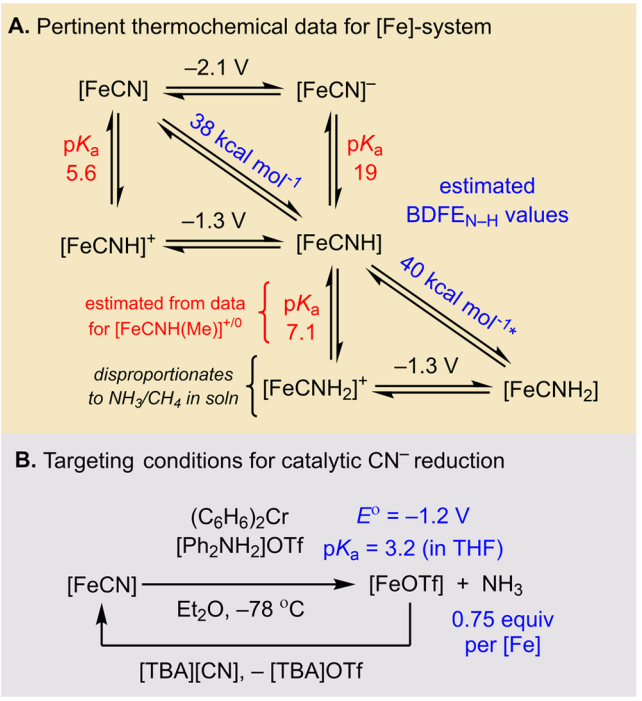

Figure 2. (A) Relevant, previously measured, thermochemical data (values in THF at 25 °C; $E°$ in referenced to $Fc^{+/0}$). (B) Exploring new conditions for the reductive protonation of [FeCN].

afforded low yields of NH_3/CH_4 (Figure 1a) despite being effective for catalytic N_2R.[38]

Curiously, in our original study, we had observed that the cationic aminocarbyne, $[FeCNH_2]OTf$, prepared via double protonation of $[FeCN][Na(12\text{-c-}4)_2]$,[25] decays upon warming to liberate 0.09 equiv NH_3/Fe and 0.07 CH_4/Fe (Figure 2), with [FeCNH]OTf and [FeOTf] as the major Fe products. This NH_3 yield represents ∼50% of that theoretically possible for a disproportionation reaction assuming a stoichiometry of five equivalents of $[FeCNH_2]OTf$ providing five H atom equivalents ($[FeCNH_2]^+ \rightarrow [FeCNH]^+ + H^+/e^-$) to reduce one equivalent $[FeCNH_2]OTf$ to NH_3 and CH_4 (eq 1).

$$6[FeCNH_2]OTf \rightarrow 5[FeCNH]OTf + [FeOTf] + NH_3 + CH_4 \quad (1)$$

Based on thermochemical data (Figure 2a),[36] removal of a H^+/e^- pair from $[FeCNH_2]^+$ is equivalent to removal of $1H^+/1e^-$ from an acid/reductant pair with $pK_a \sim 7$ and $E° \sim -1.3$ V. Reagents suiting these values would be significantly milder than $[^{2,5\text{-Cl}}PhNH_3]OTf$ and Cp^*_2Co. Hence, once $[FeCNH_2]^+$ is formed *in situ* via reductive protonation of [FeCN] (pK_a = 5.6), comparatively mild reagents should drive net CN^- reduction. Because [FeCN] can be converted to $[FeCNH_2]$-OTf with a reductant strength of $E° \approx -1.3$ V, we deduced that the $7H^+/6e^-$ reduction of [FeCN] should be accessible with reductants at $E° \approx -1.3$ V.

Gratifyingly, [FeCN] was stirred with $(C_6H_6)_2Cr$ ($E°$ = −1.2 V, Figure S23)[39] and $[Ph_2NH_2]OTf$ (pK_a 3.2)[40] in Et_2O at −78 °C and then the reaction mixture was allowed to warm to RT overnight yielding 0.75 equiv NH_3/Fe (75% yield per reductant) with [FeOTf] as the major Fe product (Figure 2b and Figure S9). Moreover, it was established that [FeOTf] reacts cleanly with excess [TBA][CN] to reform [FeCN], setting the stage for catalysis (Figure S10).

https://doi.org/10.1021/jacs.3c12395
J. Am. Chem. Soc. 2024, 146, 5343−5354

Catalytic CN^- Reduction. Thus, using [FeCN] (0.72 mM) as a precatalyst, in a reaction mixture containing 140 equiv [TBA][CN] (100 mM), 480 equiv $[Ph_2NH_2]OTf$, and 360 equiv $(C_6H_6)_2Cr$ in Et_2O at 25 °C, yielded 28 ± 5 equiv NH_3/Fe after 80 min (Figure 2c and Table 1, entry 1).

Table 1. Results for the Catalytic Reduction of CN^- to Ammonia

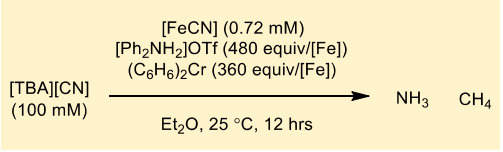

entry	change from standard conditions	NH_3 (equiv/Fe)	CH_4 (equiv/Fe)	yield per reductant (%)[a]
1	none	28 ± 5	25 ± 4	47 ± 8
2	−78 °C→25 °C	33 ± 6	33 ± 3	55 ± 10
3	−20 °C→25 °C	35 ± 8		58 ± 13
4	0 °C→25 °C	26 ± 2		43 ± 3
5	2.9 mM [FeCN][b]	9.7 ± 0.2		65 ± 1
6	0.15 mM [FeCN][b]	73 ± 4		24 ± 1
7	no [FeCN][b]	<0.4	<0.3	<1
8	no [TBA][CN][b]	0.7		1.2
9	8.0 mM $FeCl_2$ as cat.[b]	0.3		5.5
10	8.0 mM $CrCl_2$ as cat.[b]	<0.05		<1
11	2.9 mM (PhB^{iPr}_3)FeBr as cat.[b]	1.4 ± 0.7	1.0 ± 0.1	12 ± 3[c]
12	2.9 mM $(P_3^B)Fe[BAr^F_4]$ as cat.[b]	2.3 ± 0.3	1.6	15.6 ± 0.6
13	Cp_2Co instead of $(C_6H_6)_2Cr$	2.8 ± 0.8		12 ± 4
14	Cp^*_2Cr instead of $(C_6H_6)_2Cr$	13.5 ± 3		32 ± 6
15	[FeOTf] as cat.	32		53
16	reloaded catalysis[d]	4.1 ± 1.0		6.8 ± 1.7

[a]Yields assume net 6 e^- reduction to generate NH_3. [b]Catalysis initiated at −78 °C and then allowed to warm gradually to 25 °C (total reaction time of 12 h). [c]This yield includes 0.6 ± 0.2 equiv CH_3NH_2. [d]After 80 min of catalysis under standard conditions (entry 1), soluble Fe species were extracted into Et_2O and then re-exposed to the standard catalytic conditions.

Using these same catalytic conditions, we also analyzed the gaseous products. CH_4 was observed as the major reduced carbon product, with a yield of 25 ± 4 equiv of CH_4/Fe, consistent with a net $7H^+/6e^-$ reduction of CN^- (eq 2; yield based on consumed $(C_6H_6)_2Cr$ is 47 ± 8%).

$$CN^- + 7H^+ + 6e^- \rightarrow CH_4 + NH_3 \quad (2)$$

Under these conditions, trace C_2 products ethylene and ethane were also identified (0.4 equiv C_2H_4 and 0.3 equiv C_2H_6 per Fe). These products correspond to $10H^+/8e^-$ and $12H^+/10e^-$ reductions of CN^-. Combined, these C_2 evolving reactions accounted for less than 2% of the consumed reductant. Hence, the [FeCN] catalyst is nearly quantitatively selective for C_1 products, as is observed via the nitrogenase enzyme.[6,7] H_2 accounts for most of the remaining reducing equivalents (yield based on $(C_6H_6)_2Cr$: 29 ± 11%). Neither CH_3NH_2 ($4e^-$ product) or CH_2NH ($2e^-$) was detected, regardless of initial temperature, using [FeCN] as a catalyst.

Curiously, whereas synthetic iron catalysts for N_2R have shown highest efficiency at low temperatures due to mitigated HER (hydrogen evolution reaction) and entropically favored N_2 binding,[41] no such advantage is observed for catalytic cyanide reduction by [FeCN] (entries 2−4). Instead, background HER via the combination of this reductant and acid is comparatively slow (*vide infra*). Also, CN^- binds favorably to [Fe(II)] at RT. For reactions started at −78 °C, catalytic turnover is slow, reflecting a slow OTf^- for CN^- metathesis step needed to turn the system over (*vide infra*); most of the observed catalysis occurs as the reaction is warmed. For a catalytic reaction run at −20 °C and quenched after 20 min, 1.7 equiv of NH_3 was detected, demonstrating that catalytic turnover occurs at this temperature but is relatively slow.

Increasing the catalyst loading to 2.9 mM (entry 5) modestly increased the NH_3 yield relative to reductant present (65 ± 1%). Lowering the catalyst loading (0.15 mM; entry 6) improved the TON for produced NH_3 (73 ± 4 equiv) but led to a corresponding drop in yield per $(C_6H_6)_2Cr$ (24 ± 1%).

A catalyst-free reaction yielded no detectable NH_3, CH_4, or other gaseous carbon products (entry 7). This conclusion is further supported by experiments with $[TBA][^{13}CN]$ as the cyanide source. ^{13}C NMR spectroscopy of catalytic runs using $[TBA][^{13}CN]$ confirmed the formation of $^{13}CH_4$ and consumption of $^{13}CN^-$ (Figures S5 and S6). By contrast, a corresponding catalyst-free reaction (under otherwise identical conditions) showed negligible consumption of $^{13}CN^-$ and no observable $^{13}CH_4$. These observations collectively establish that the Fe catalyst is required for consumption of substrate and responsible for the NH_3 and CH_4 products.

Catalysis run in the absence of [TBA][CN] produced 0.7 equiv of NH_3, with $[FeC^{15}N]$ used to demonstrate that this NH_3 arose solely from precatalyst reduction and not N_2R (entry 8, Figure S4).

The nature of the phosphine-ligated iron catalyst appears to be critical. $FeCl_2$ instead of [FeCN] produced only 0.3 equiv of NH_3 under the standard conditions (entry 9), and $CrCl_2$ instead of [FeCN] produced no detectable NH_3 (entry 10). The tris(phosphino)iron complexes $(P_3^B)Fe[BAr^F_4]$[16] and $(PhBP^{iPr}_3)FeBr$[42] (P_3^B represents a trisphosphine borane ligand; $PhBP^{iPr}_3$ represents a trisphosphine borate ligand) showed very moderate activity as (pre)catalysts compared to [FeCN] (entries 11−12). Curiously, for $(PhBP^{iPr}_3)FeBr$, a small amount of methylamine, CH_3NH_2 (0.6 ± 0.2), was detected as a product. These iron phosphine precatalysts produce CH_4 as the major hydrocarbon product but with a lower selectivity. The ratio of C_2/C_1 products produced is 0.16 and 0.11 for $(P_3^B)Fe[BAr^F_4]$ and $(PhBP^{iPr}_3)FeBr$, respectively (Table S3), compared to 0.02 for [FeCN].

While $(C_6H_6)_2Cr$ is the favored reductant for CN^- reduction, other reductants including Cp_2Co ($E° = -1.3$ V, Figure S25; entry 13) and Cp^*_2Cr ($E° = -1.5$ V, Figure S27; entry 14) were modestly competent. The low yields for these reductants do not appear to correlate with the reduction potential of the chemical reductant. Instead, we attribute the strong attenuation in yield to enhanced background HER. Accordingly, we find that the rate of reaction of each reductant independently with $[Ph_2NH_2]OTf$ (to produce H_2), as measured by cyclic voltammetry, inversely correlates with the NH_3 TON observed in a catalytic run when CN^- is present under the standard conditions (see Section S8.2 for details).

To summarize, we have established a highly selective catalytic system for NH_3 and CH_4 production via reductive protonation of CN^-; the choice of catalyst ([FeCN]) and reductant ($(C_6H_6)_2Cr$) is crucial for observing high turnover and significant yields.

https://doi.org/10.1021/jacs.3c12395
J. Am. Chem. Soc. 2024, 146, 5343−5354

Mechanistic Studies. Scheme 1 provides a working outline for the catalytic CN^- reduction cycle starting from

Scheme 1. Proposed Mechanism for CN^- Reduction to NH_3 and CH_4 as Catalyzed by [FeCN]

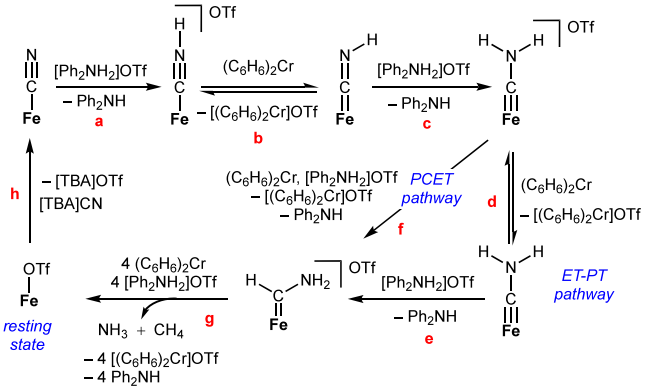

[FeCN], emphasizing the early intermediates of the cycle. To guide the following discussion, summary remarks concerning a plausible pathway are as follows: [FeCN] is first protonated (step a) to form independently characterized $[FeCNH]^+$,[25] which is then reduced (to [FeCNH]; step b) and protonated (step c) to afford the independently characterized amino-carbyne, $[FeCNH_2]^+$.[25] $[FeCNH_2]^+$ is in redox equilibrium with $[FeCNH_2]$ in the presence of $(C_6H_6)_2Cr$ (step d). These carbyne intermediates are suggested to be rate-contributing to overall CN^- reduction (see below). Along the ET-PT pathway, $[FeCNH_2]$ can be protonated to form a posited carbene intermediate (step e), $[FeC(H)(NH_2)]^+$. This carbene is modeled via the independent generation of its methylated analogue, $[FeC(H)(NMe_2)]^+$, via the protonation of $[FeCNMe_2]$ (see below). This observation and computational evidence each lends support to C–H bond formation to produce $[FeC(H)(NH_2)]^+$ during catalysis. A direct PCET pathway from $[FeCNH_2]^+$ to $[FeC(H)(NH_2)]^+$ is also plausible (step f). Finally, a series of downstream (as yet undefined), facile reductive protonation steps of $[FeC(H)(NH_2)]^+$ are proposed to release NH_3 and CH_4 along with [FeOTf] (step g); the latter is returned to [FeCN] via metathesis with [TBA][CN], a step (step (h)) that is turnover limiting.

Probing Catalyst Resting State and Deactivation. To probe speciation during catalysis, we prepared $[^{57}FeCN]$ to facilitate monitoring the catalysis by ^{57}Fe Mössbauer spectroscopy via low-temperature quenching of catalytic runs initiated at 25 °C. Related studies proved insightful for N_2R catalysis by related Fe systems.[40,43]

Freeze-quenching (77 K) the catalysis after 1 min at 25 °C, we found $[^{57}FeOTf]$ as the sole iron species present (see Section S6.2).[44] This result points to [FeOTf] as the catalyst resting state with metathesis step (h) being turnover limiting. Consistent with this observation, [FeOTf] performs analogous to [FeCN] as a catalyst (Table 1, entry 15). Freeze-quenched snapshots at later reaction times show attenuation in the signal for $[^{57}FeOTf]$ and the growth of unknown iron species. After 80 min, all of the $[^{57}FeOTf]$ has been consumed; the remaining iron species showed poor activity following extraction and (re)subjection to catalytic conditions at 25 °C with fresh acid, reductant and [TBA][CN], yielding only an additional 4.1 ± 1 equiv NH_3 (entry 16). NMR analysis of the postcatalysis mixture revealed evidence of a diamagnetic iron hydride (possibly $[Fe(H)(NHPh_2)]$) with the $(P_3^{Si})Fe$ platform intact, as well as free $Si(H)P_3$ (Figure S13). Relatedly, iron hydrides (e.g., $[Fe(H)(N_2)]$) have been shown to be off-cycle sinks during catalytic N_2R.[43,45,46]

While our mechanistic studies have focused on the most efficient catalyst, [FeCN], initial studies of the reactivity of $(P_3^B)Fe[BAr^F{}_4]$ and $(PhBP^{iPr}{}_3)FeBr$ suggest that these less efficient precatalysts are also less stable to excess CN^-. When reacted with 20 equiv [TBA][CN] in Et_2O (in the absence of acid or reductant), free phosphine is observed, indicating partial demetalation as a pathway for deactivation, offering a plausible reason for the lower turnover numbers (Figures S14 and S15).

Early N–H Bond Forming Steps. Since metathesis to produce [FeCN] from [FeOTf] appeared to be turnover limiting, we turned to stoichiometric experiments to probe the role(s) of early intermediates of reductive protonation in this catalysis.

Exposing a solution containing a mixture of [FeCN] and a large excess (20 equiv) of $(C_6H_6)_2Cr$ (unreactive in the absence of acid) to $[Ph_2NH_2]OTf$ (20 equiv, added via a syringe) caused distinct color changes that could be monitored by UV–vis spectroscopy (Figure 3). While higher energy

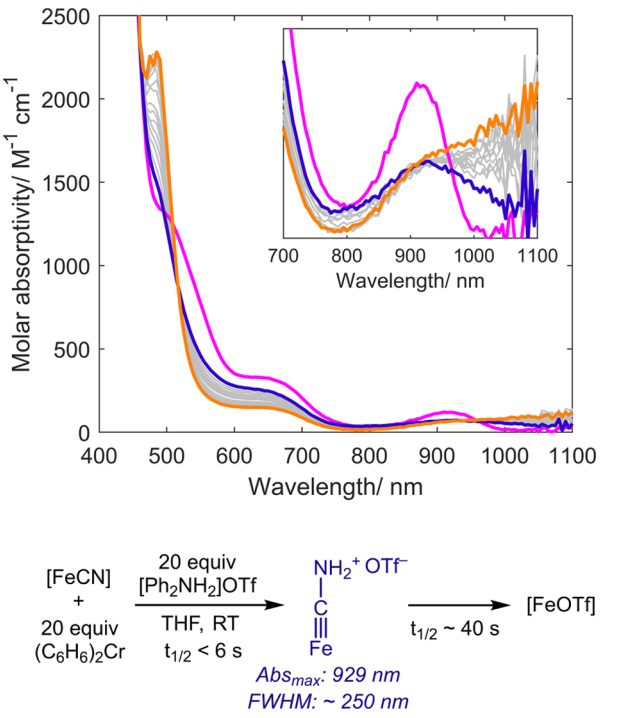

Figure 3. UV–vis data showing the *in situ* formation of $[FeCNH_2]$-OTf (blue trace, 6 s after acid addition) in the reduction of [FeCN] (pink trace) to [FeOTf] (orange trace, 240 s after acid addition).

absorptions (λ < 600 nm) are complicated by the absorption spectrum of $(C_6H_6)_2Cr^{+/0}$, the lower energy transitions provide a useful handle for the iron speciation. Upon addition of the acid (all 20 equiv) at RT, the characteristic near-IR absorption of [FeCN] (λ_{max} = 905 nm, FWHM ≈100 nm; pink trace) decayed rapidly ($\tau_{1/2}$ < 6 s) and a new, broader absorbance characteristic of $[FeCNH_2]^+$ (λ_{max} = 929 nm, FWHM ≈250 nm; blue trace) was observed.[25] This feature decayed more slowly ($\tau_{1/2}$ ~ 40 s under the conditions studied) with

https://doi.org/10.1021/jacs.3c12395
J. Am. Chem. Soc. 2024, 146, 5343–5354

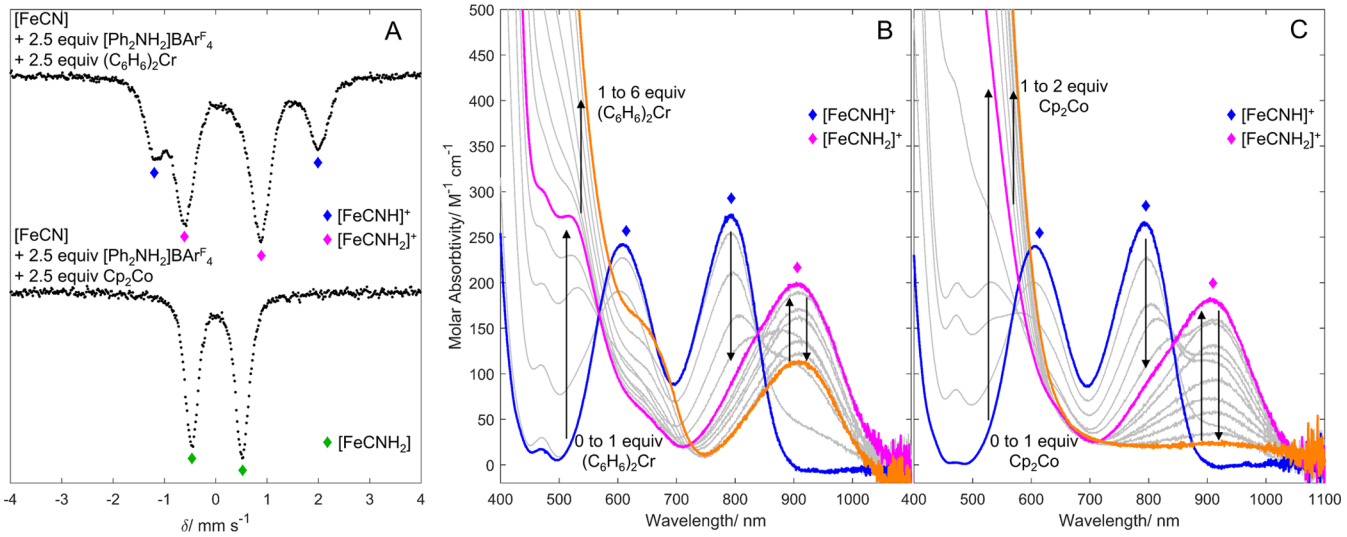

Figure 4. (A) ^{57}Fe Mössbauer spectra of reaction of [FeCN] with $[Ph_2NH_2]BAr^F_4$ and $(C_6H_6)_2Cr$ or Cp_2Co. (B, C) UV−vis data for reaction of [FeCN] with $[Ph_2NH_2]BAr^F_4$ and $(C_6H_6)_2Cr$ (B) or Cp_2Co (C) to form early intermediates $[FeCNH]BAr^F_4$ (blue trace), $[FeCNH_2]BAr^F_4$ (pink trace), and $[FeCNH_2]^0$ (orange trace).

simultaneous growth of a shoulder that extends further into the near-IR, and a strong absorption centered at 485 nm (orange trace). These latter features are consistent with the formation of [FeOTf], as was also confirmed by ^{1}H NMR spectroscopy (Figure S12). Products were also analyzed (1.0 equiv of NH_3/Fe and 0.9 equiv CH_4/Fe). These data demonstrate the aminocarbyne $[FeCNH_2]^+$ as an observable on-path intermediate in the conversion of [FeCN] to [FeOTf]. Isosbestic points at 520 and 900 nm establish that no further downstream intermediates buildup as $[FeCNH_2]^+$ is converted to [FeOTf] during liberation of NH_3 and CH_4.

To interrogate shorter-lived intermediates, we next studied the consumption of [FeCN] at lower temperature, using fewer equivalents of reductant and acid. Mixing [^{57}FeCN] with $[Ph_2NH_2]BAr^F_4$ and $(C_6H_6)_2Cr$ (2.5 equiv each) in Et_2O at −78 °C for 1 min, followed by freeze-quench (77 K) and analysis by Mössbauer spectroscopy, showed primarily $[^{57}FeCNH_2]BAr^F_4$ (Figure 4a; δ = 0.13 mm s^{-1} and ΔE_Q = 1.47 mm s^{-1}), again supporting the proposed intermediacy of $[FeCNH_2]^+$ during catalysis.[25] These low-temperature conditions also allowed identification of the first intermediate of protonation, $[^{57}FeCNH]BAr^F_4$ (δ = 0.407 mm s^{-1} and ΔE_Q = 3.20 mm s^{-1}),[25] as a minor component, consistent with step (a) (Scheme 1).

We also obtained evidence for a facile redox equilibrium between $[FeCNH_2]^{+/0}$ and $(C_6H_6)_2Cr^{+/0}$, as can be expected based on the estimated difference in their reduction potentials ($E°(Fe^{+/0}) \sim -1.2$ V, $E°(Cr^{+/0}) = -1.2$ V; see Section S8.3 for data). Relatedly, the available data imply that single electron reduction of $[FeCNH_2]^+$ to $[FeCNH_2]$ (step d) is feasible under conditions relevant to the catalysis. Accordingly, addition of 2.5 equiv of $[Ph_2NH_2]BAr^F_4$ to a THF solution of [FeCN] at −80 °C resulted in the immediate formation of $[FeCNH]BAr^F_4$ (Figure 4b, blue trace).[25,47] Following this, the solution was titrated with 0−6 equiv of $(C_6H_6)_2Cr$ to study its response (Figure 4b). During the addition of the first equivalent of $(C_6H_6)_2Cr$, UV−vis maxima for $[FeCNH]^+$ (800 and 610 nm) decreased in intensity and new maxima appeared, reflecting the growth of $[FeCNH_2]^+$ (929 and 570 nm; pink trace). Isosbestic points at 570 and 860 nm establish no other intermediate buildup. Upon addition of further equivalents of $(C_6H_6)_2Cr$, the signals for $[FeCNH_2]^+$ attenuate with corresponding growth of a strong absorbance with a shoulder at around 560 nm (orange trace). These changes are consistent with the reduction of $[FeCNH_2]^+$ to $[FeCNH_2]$. Still, even after addition of 6 equiv $(C_6H_6)_2Cr$, a large fraction of $[FeCNH_2]^+$ remained.[48] These results confirm a redox equilibrium between $[FeCNH_2]^{+/0}$ and $(C_6H_6)_2Cr^{+/0}$ (step (d)).

As expected for such a redox equilibrium, cobaltocene, a stronger reductant than $(C_6H_6)_2Cr$ ($E°(Cp_2Co^{3+/2+}) = -1.3$ V), completely reduces $[FeCNH_2]^+$ to $[FeCNH_2]$. Accordingly, ^{57}Fe Mössbauer spectra of the reaction between [^{57}FeCN] with $[Ph_2NH_2]BAr^F_4$ and Cp_2Co (2.5 equiv each) at −78 °C in Et_2O reveal the formation of a single new species (δ = 0.02 mm s^{-1} and ΔE_Q= 0.99 mm s^{-1}; Figure 4a). These parameters closely resemble those of $[FeCNMe_2]$ (δ = 0.06 mm s^{-1} and ΔE_Q= 1.12 mm s^{-1}),[25] consistent with formation of $[FeCNH_2]$. Complete formation of $[FeCNH_2]$ with only 2.5 equiv of reductant differs markedly from conditions using $(C_6H_6)_2Cr$. Titrations monitored by UV−vis spectroscopy using Cp_2Co still showed $[FeCNH_2]^+$ as an intermediate upon addition of just 1 equiv of Cp_2Co to a mixture of [FeCN] and $[Ph_2NH_2]BAr^F_4$ (Figure 4c, pink trace). Upon addition of a second equiv of Cp_2Co, $[FeCNH_2]^+$ is fully consumed with concomitant formation of $[FeCNH_2]$ (orange trace).

Evidence for C−H Bond Formation via Fe═C(H)NH$_2^+$. The intermediacy of iron carbynes $[FeCNH_2]^{+/0}$ in catalytic CN^- reduction corresponds to the intermediacy of isolobal hydrazidos $[FeNNH_2]^{+/0/-}$, during Fe-catalyzed N_2R.[27−29,49,50] With this analogy in mind, we wondered whether iron carbynes might be selectivity determining in CN^- reduction, with final N−H bond formation releasing NH_3 (analogous to N_β−H bond formation in N_2R via hydrazido intermediates), resulting in the observed 6 e$^-$ products (CH_4 and NH_3), possibly via a transient carbide [Fe(C)] intermediate. Computational evidence and a study of the reactivity of the methylated carbyne $[FeCNMe_2]$ complex instead support the formation of a C−H bond via a carbene intermediate, $[Fe═C(H)(NH_2)]^+$, as the next step of the

https://doi.org/10.1021/jacs.3c12395
J. Am. Chem. Soc. 2024, 146, 5343−5354

cycle. This path implies that the aminocarbyne is not selectivity determining in the present system; C−N bond cleavage occurs later in the catalytic cycle.

As intermediates downstream of $[FeCNH_2]$ cannot be identified during the CN^- reduction process, we studied the reactivity of the more tractable, methylated $[FeCNMe_2]$ analogue (Scheme 2). Thus, a reaction between $[FeCNMe_2]$

Scheme 2. Protonation and Proton-Coupled Reduction of $[FeCNMe_2]$ as a Model of $[FeCNH_2]$ Reactivity

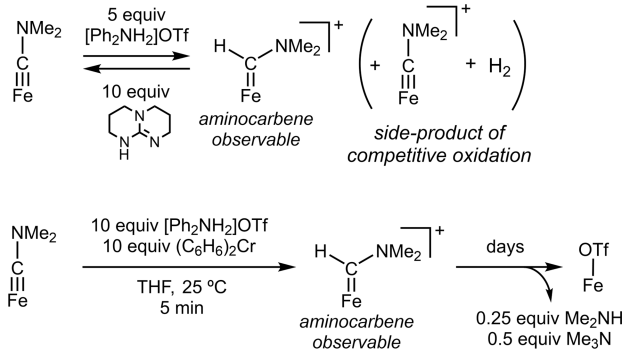

and $[Ph_2NH_2]OTf$ in the absence of added reductant affords a new paramagnetic species, observed via UV−vis and ^1H NMR spectroscopy (see SI, Section S9); some competing oxidation to $[FeCNMe_2]^+$ (with loss of H_2) is also observed in the reaction mixture, frustrating isolation and purification of the new species. Nonetheless, on the basis of reactivity and ^{57}Fe Mössbauer (*vide infra*), we assign the product of protonation as the aminocarbene $[FeC(H)(NMe_2)]^+$. Its formation is reversible; $[FeCNMe_2]$ is cleanly regenerated upon addition of a triazabicyclodecene (TBD) base (Scheme 2 and Figure S32).

$[FeCNMe_2]$ also reacts with 10 equiv $[Ph_2NH_2]OTf$ in the presence of 10 equiv $(C_6H_6)_2Cr$ in THF at room temperature and is gradually converted to [FeOTf] over a period of 7 days, with Me_2NH (0.25 equiv) and (curiously) Me_3N (0.5 equiv) detected as the N-containing products.[51] Notably, we had previously observed that $[FeCNMe_2]$ is not reduced in combination with Cp^*_2Co and $[^{2,5\text{-Cl}}PhNH_3]OTf$.[25]

While formation of [FeOTf] from $[FeCNMe_2]$ is slow in the presence of $[Ph_2NH_2]OTf$ and $(C_6H_6)_2Cr$ (at 10 equiv each), the $[FeCNMe_2]$ is consumed rapidly ($\tau_{1/2} \approx 1$ min at 25 °C) and the same paramagnetic (presumed) carbene species is now also observed as an intermediate. Hence, reacting $[FeCNMe_2]$ with excess $(C_6H_6)_2Cr$ and $[Ph_2NH_2]OTf$ and freeze-quenching the reaction after 5 min revealed a new major species with the Mössbauer parameters $\delta = 0.40$ mm s^{-1} and $\Delta E_Q = 2.25$ mm s^{-1} (Figure S37), consistent with an $S = 1$ $[FeC(H)(NMe_2)]^+$ species with parameters similar to previously characterized $S = 1$ $(P_3^{Si})Fe^{II}–L^+$ species (L = CO, CNR or N_2).[36,52] Taken together, these data are highly consistent with $[FeC(H)(NMe_2)]^+$ as an intermediate during the reductive protonation of $[FeCNMe_2]$ to liberate [FeOTf] and the amine products and suggest that $[FeC(H)(NH_2)]^+$ would form readily via protonation of $[FeCNH_2]$ during CN^- reduction catalysis.

To gain further support for this proposed $[Fe{=}C(H)(NH_2)]^+$ intermediate, we turned to computational methods to explore the energy of aminocarbene species versus other plausible isomers. The TPSS functional[53] and a def2-TZVP basis set on Fe, with a def2-SVP basis set on all other atoms,[54] reliably replicate experimentally estimated BDFEs for complexes similar to those discussed here.[55] We thus used this approach to compare plausible isomers with specified spin states under the addition of H$^\bullet$ to the $[FeCNH_2]^{+/0}$ carbynes (Figure 5a). We find that iron carbenes $[Fe{=}C(H)(NH_2)]^{+/0}$

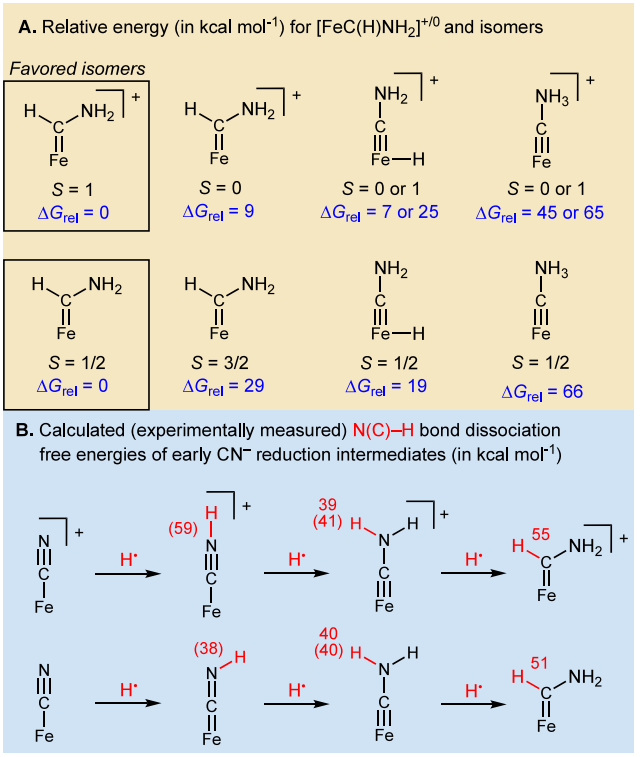

Figure 5. (A) Comparing the energies of isomers in specified spin states for $[FeC(H)(NH_2)]^{+/0}$. (B) Calculated N−H bond and C−H bond dissociation free energies (BDFEs). Experimentally determined values are provided in parentheses; for carbynes, these are estimated from $[FeCN(H)(Me)]^{+/0}$.[36]

in their corresponding $S = 1$ and $S = 1/2$ spin states, respectively, are the lowest energy isomers ($\Delta G_{rel} = 0$ kcal mol^{-1}) when compared to their corresponding ammonium carbyne isomers ($[Fe{\equiv}C–NH_3]^{+/0}$; $\Delta G_{rel} = 45–66$ kcal mol^{-1}) and iron carbyne hydrides ($[(H)Fe{\equiv}C–NH_2]^{+/0}$; $\Delta G_{rel} = 7–25$ kcal mol^{-1}). Alternative spin states of the iron carbenes (S = 0 or 3/2) are also higher in energy ($\Delta G_{rel} = 9$ and 29 kcal mol^{-1}, respectively). The small ΔG_{rel} of $[(H)Fe{\equiv}C–NH_2]^+$ is interesting given that iron hydrides can be catalytic sinks for this system;[46] isomerization between the on-path iron carbene and this iron carbyne hydride might be a relevant deactivation pathway.

The thermodynamic favorability of C−H bond formation (over N−H bond formation) can be rationalized by considering the basicity of the N and C atoms of the iron aminocarbyne. $[FeCNH_2]$ features a planar sp^2-hybridized N atom, suggesting substantial π donation from N, which can be expected to make the N atom less basic than the carbyne C atom. Such a scenario would favor C atom protonation as observed.

Computationally, the carbene $[FeC(H)(NH_2)]^{+/0}$ C−H bonds (51−55 kcal mol^{-1}) are much stronger than the carbyne $[FeCNH_2]^{+/0}$ N−H bonds (39−40 kcal mol^{-1}; Figure 5b), consistent with the conversion of carbyne to carbene being a thermodynamically favorable step in [FeCN] reduction

https://doi.org/10.1021/jacs.3c12395
J. Am. Chem. Soc. 2024, 146, 5343−5354

(Figure 6). However, the buildup of $[FeCNH_2]^+$ as an observable intermediate when [FeCN] is reduced to NH_3 and

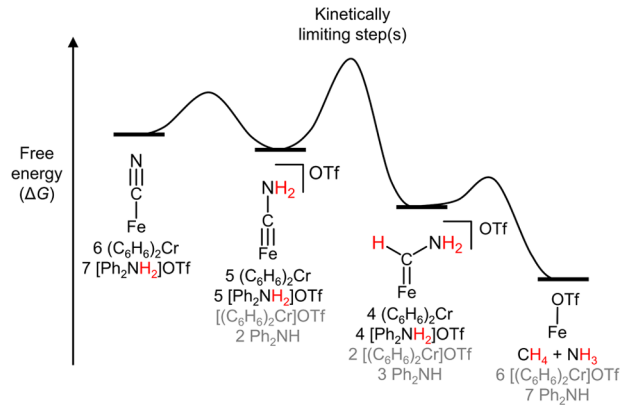

Figure 6. Proposed qualitative energy barriers for transformation of [FeCN] to [FeOTf] with key intermediates, $[FeCNH_2]^+$ and $[FeC(H)(NH_2)]^+$ indicated.

CH_4 (Figure 3), and the slow protonation observed for $[FeCNMe_2]^0$ (Scheme 2) suggests a significant kinetic barrier in converting $[FeCNH_2]^{+/0}$ to $[FeC(H)(NH_2)]^{+/0}$ (Figure 6). This can be rationalized by a rehybridization at carbon with a corresponding change in spin state upon protonation, which would correlate with a significant kinetic barrier.

DISCUSSION

Comparison to Other Fe-Based Catalysts. As introduced above, reported Fe catalysts for cyanide (or HCN) reduction have exclusively been Fe−S clusters, as either the protein active sites of nitrogenase enzymes,[5−9,13] the extracted cofactors (e.g., FeMoco),[10−12] or synthetic clusters.[20−22] The extracted cofactors and synthetic clusters studied have been shown to reduce CN^- using weak acids (lutidinium or pH 8 buffered solutions) and lanthanide(II) reductants (SmI_2 or Eu^{II}(DTPA)) as a source of H^+/e^- equivalents. Invariably, these systems have produced substantial amounts of C_{2+} products, accounting for 20−40% of the total reduced carbon products, in addition to C_1 products, including CH_4 (and NH_3) or CH_3NH_2.[10−12,20−22]

By contrast, the [FeCN] catalyst studied herein shows <2% C_{2+} products. Curiously, its reactivity profile more closely resembles that of HCN reduction by MoFe nitrogenase, where C_{2+} products account for <0.1% of the total reduced carbon.[6,7] Still, [FeCN] shows much higher selectivity for the 6 e^- reduction products (CH_4 + NH_3) than has been observed for the nitrogenases studied (MoFe and VFe variants), which also show significant CH_3NH_2 production (MoFe, CH_3NH_2:CH_4 = 0.39; VFe, CH_3NH_2:CH_4 = 0.66−1.1).[9] The complex $(PhBP^{iPr}_3)$FeBr, while a less active catalyst system for CN^- reduction (Table 1, entry 10), more faithfully captures the selectivity of nitrogenases, producing substantial CH_3NH_2 as well as (CH_4 + NH_3). As functional models, the (P_3^B)Fe− and (P_3^{Si})Fe−systems we have studied are distinct in that both have been shown to display catalytic activity for N_2R and CN^- reduction, akin to ATP-dependent nitrogenase enzymes.[1,5,16,43]

Mechanistic Findings. The data presented above allow us to posit several important intermediates we believe to be on the path for catalytic CN^- reduction by [FeCN] (Scheme 1) and to further consider the observed selectivity. A key observation from low-temperature UV−vis titrations includes the finding that [FeCN] is readily protonated by $[Ph_2NH_2]$-OTf. The resulting isocyanide $[FeCNH]^+$ can be reduced by $(C_6H_6)_2Cr$, and the resulting $[FeCNH]^0$ product is rapidly protonated to afford the observable aminocarbyne $[FeCNH_2]^+$. With $(C_6H_6)_2Cr$ present as the reductant, $[FeCNH_2]^+$ and $[FeCNH_2]$ were shown to be in redox equilibrium.

While we observe downstream conversion of $[FeCNH_2]^+$ to [FeOTf] at room temperature (associated with liberation of NH_3 and CH_4), we have been unable to characterize intermediates of this transformation even at low temperature. However, by reconciling computational data with the observed reactivity of a methylated analogue, $[FeCNMe_2]$, we favor a C−H bond forming step to produce $[FeC(H)(NH_2)]^+$ as the next intermediate from $[FeCNH_2]^+$ along the catalytic pathway, possibly via ET-PT (steps d and e in Scheme 1) or PCET (step f). This Fischer-type aminocarbene would plausibly be on the path for either CH_4 + NH_3 (6 e^-), or CH_3NH_2 (4 e^-), products. The selectivity determining C−N bond cleaving step that produces the 6 e^- products in this system must therefore occur at a later stage of the catalytic cycle, with additional (and facile) $4H^+/4e^-$ transfers (Scheme 1, step g).

From the Fischer carbene (or its one-electron reduced congener), several pathways can account for CH_4 and NH_3 products (depicted in Figure 7a). Guided by theoretical studies, we can, qualitatively at least, compare them. Ultimately, each specific H^+ and e^- step likely needs to be examined to fully account for CH_4 and NH_3/CH_3NH_2 selectivity, as has been the case for NH_3/N_2H_4 selectivity during N_2R (Figure 7b).[28,29,50] However, acknowledging increased error in theoretical calculations when studying changes in charge state,[56] we have opted to limit our present considerations to the thermodynamics of the addition of a net H atom to $[FeC(H)_x(NH_2)]^{+/0}$ (x = 1, 2) species, and the associated C−N bond strengths of the ammonium intermediates, $[FeC(H)_x(NH_3)]^{+/0}$, that form. The combined H^+/e^- transfers (Figure 7a) are referenced to the combination of $(C_6H_6)_2Cr$ (e^-) and $[Ph_2NH_2]$OTf (H^+; see the SI for details).

We consider three pathways in Figure 7a(i−iii) as an expansion on step g introduced in Scheme 1. Pathways i−iii proceed via either cationic or neutral intermediates, and we use +/0 to differentiate between these charge states in the figure.

Starting from the aminocarbene +/0 intermediates, addition of the next H^+/e^- equivalent at N would yield an ammonium carbene, $[FeC(H)(NH_3)]^{+/0}$, which could liberate NH_3 and an iron methylidyne, $[Fe{\equiv}C-H]^{+/0}$. The methylidyne is envisioned to be reductively protonated to form CH_4 and [FeOTf] (Figure 7a, pathway i). The plausibility of iron methylidyne intermediacy in this P_3^{Si}Fe catalyst system is supported by our recent report of the isolation and structural characterization of the methylated analogues $[P_3^{Si}Fe{\equiv}C-CH_3]^{+/0}$.[44]

Alternatively, C−H instead of N−H bond formation from $[FeC(H)(NH_2)]^{+/0}$ would yield an iron alkylamine product. We consider computationally such a species as two spin-isomers, a low spin (S = 0, 1/2) η^2-iminium adduct ($[Fe(\eta^2-CH_2NH_2)]^{+/0}$) and an intermediate spin (S = 1, 3/2) η^1-alkylamine ($[Fe(\eta^1\text{-}CH_2NH_2)]^{+/0}$). In $[Fe(\eta^1\text{-}CH_2NH_2)]^{+/0}$ intermediates, N−H bond formation is likely kinetically favorable (see below), but from the η^2-iminium adduct, we

https://doi.org/10.1021/jacs.3c12395
J. Am. Chem. Soc. 2024, 146, 5343−5354

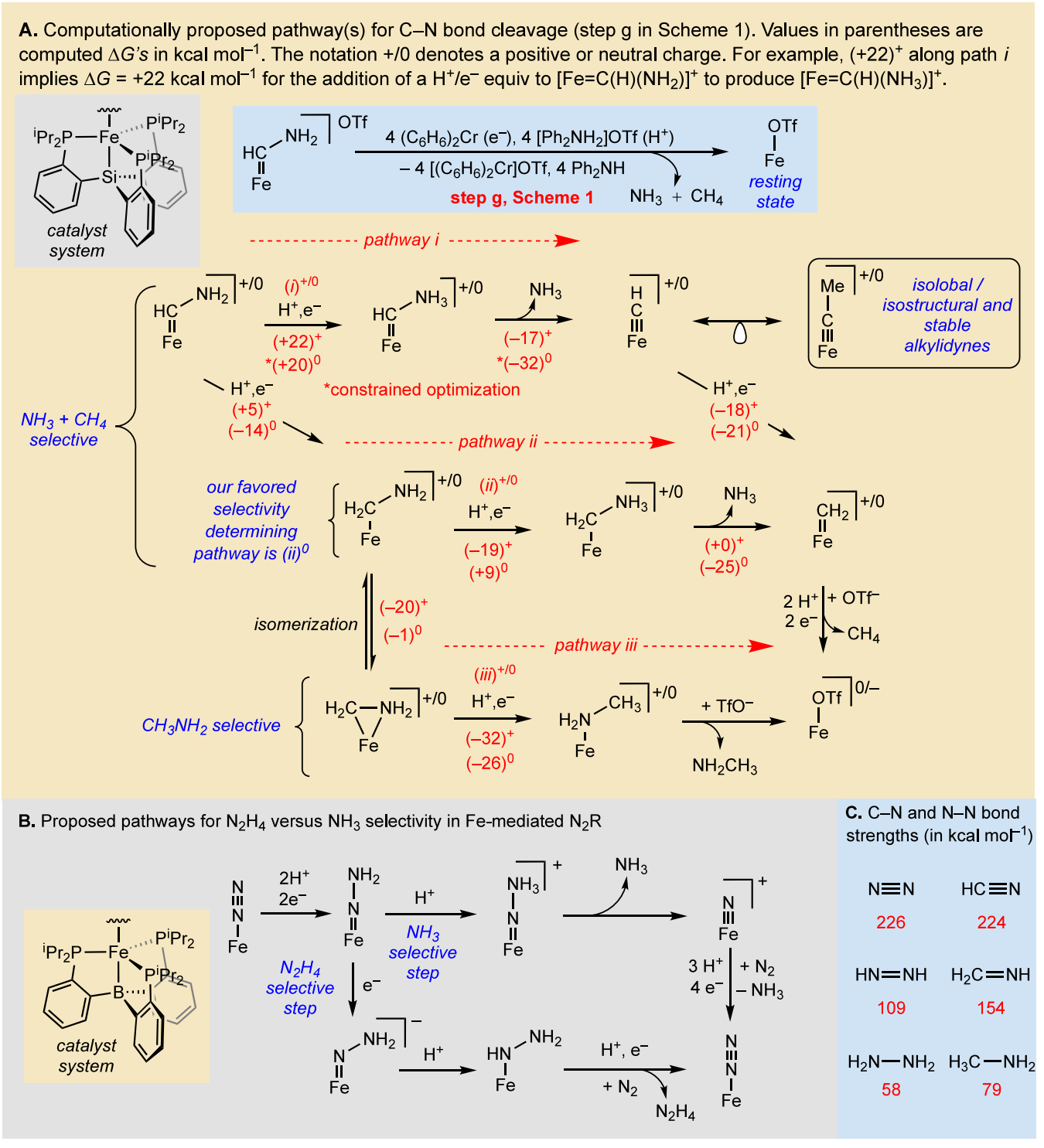

Figure 7. (A) Plausible pathways *i*–*iii* for C–N bond cleavage via step g in Scheme 1 for CN^- reduction by the $P_3^{Si}Fe$ system, attempting to rationalize selectivity, with associated thermodynamic data for stepwise e^-/H^+ transfers en route to product, with values for both cationic (+) and neutral (0) species. Pathway ii^0 is our favored pathway. (B) Comparison with N–N bond cleavage in Fe-mediated N_2R by the P_3^BFe-system, accounting for NH_3 versus N_2H_4 selectivity. (C) Comparison of N–N and C–N bond strengths in N_2 and HCN and their further reduced derivatives.[61]

anticipate similar barriers for C–H and N–H bond formation. From either alkylamine isomer, N–H bond formation would yield the alkylammonium product $[FeC(H)_2(NH_3)]^{+/0}$ (pathway *ii*). C–N bond cleavage releases NH_3 and an iron methylidene ($[Fe{=}CH_2]^{+/0}$). While we have not previously characterized a terminal $P_3^{Si}Fe{=}CR_2$ carbene (for R = H or alkyl), cationic, diamagnetic iron methylidenes, $[CpFe(L_2){=}CH_2]^+$ (L = phosphine or CO), have been synthesized by O atom protonation of a corresponding methoxymethyl iron complex, followed by C–O bond cleavage.[57−59] Such a scenario is akin to the C–N bond cleavage suggested here. Addition of a further $2H^+/2e^-$ releases CH_4 from $[FeCH_2]^{+/0}$.

https://doi.org/10.1021/jacs.3c12395
J. Am. Chem. Soc. 2024, 146, 5343−5354

A CH_3NH_2 selective pathway, $(iii)^{+/0}$, has also been considered, where the addition of H^+/e^- to the C atom of $[Fe(\eta^2\text{-}CH_2NH_2)]^{+/0}$ results in a methylamine adduct, $[FeNH_2CH_3]^{+/0}$. The latter should readily liberate CH_3NH_2 upon reduction, as has been demonstrated for the ammonia-complex, $[P_3^{Si}FeNH_3]^+$.[60]

Computational analysis of the intermediates along these three pathways shows that the C−H bond formation is always thermodynamically favored. Consequently, if the strongest bond is always formed, CN^- reduction would produce CH_3NH_2 instead of CH_4 and NH_3 (Figure 7; pathway *iii*). Hence, to account for the observed CH_4 and NH_3 products, we propose that the bulky ^{i}Pr-groups on the P_3^{Si} ligand limit access to the carbyne C atom and thereby kinetically favor N−H bond formation. This leads to ammonium intermediates $[FeC(H)_x(NH_3)]^{+/0}$ (x = 1,2) that ultimately liberate NH_3 (and then CH_4; Figure 7, pathways *i* and *ii*). This rationalization accommodates the observed mixture of CH_3NH_2 and NH_3 observed when using $(PhBP^{iPr}_3)FeBr$ as a catalyst instead of [Fe] (Table 1, entry 10); the 4-coordinate Fe center in $(PhBP^{iPr}_3)FeBr$ affords a more accessible carbyne intermediate C atom.[62] Accordingly, the rate of C−H bond formation can compete with N−H bond formation and CH_3NH_2 is an observable product. Relatedly, we suspect that the increased steric bulk at N in $[FeCNMe_2]$ slows the rate of N−H bond formation, leading to the observed product distribution (2:1 Me_3N:Me_2NH).

With these considerations, we next compared the NH_3/CH_4 selective pathways (*i* and *ii*). We favor pathway $(ii)^0$ as a pathway involving exothermic and mildly endergonic steps, with C−N bond cleavage occurring from $[FeCH_2NH_3]^0$. Considering pathways $(i)^{+/0}$, they feature highly endergonic N−H bond formation steps (+22 and +20 kcal mol^{-1}, respectively). As this step is followed by exothermic C−N bond cleavage and reductive protonation of the resulting methylidyne, pathways $(i)^{+/0}$ may nevertheless be kinetically competent.[63] Path $(ii)^+$ features downhill or mildly endergonic steps. We nevertheless disfavor this pathway (compared to $(ii)^0$) due to the high favorability of the diamagnetic $[Fe(\eta^2\text{-}CH_2NH_2)]^+$ (−20 kcal mol^{-1} compared to $[Fe(\eta^1\text{-}CH_2NH_2)]^+$), with subsequent H$^\bullet$ addition at C rather than N being very exothermic from $[Fe(\eta^2\text{-}CH_2NH_2)]^+$.

Our favored path $(ii)^0$ points to a selectivity determining step at the addition of a (net) H$^\bullet$ to $[Fe(\eta^1\text{-}CH_2NH_2)]^0$; the latter constitutes a $4H^+/4e^-$ intermediate of [FeCN] reduction. By contrast, the proposed selectivity determining intermediate during N_2R is $[FeNNH_2]$, a $2H^+/2e^-$ intermediate (Figure 7b). Compared to isolobal N≡N, C≡N$^-$ requires a greater degree of reduction before the C−N bond cleavage can occur. This is consistent with the respective C−N and N−N σ bond strengths: While their triple bond strengths are similar, the bond weakening upon decrease in bond order is much greater for N_2 (Figure 7c).[61]

In addition to the high selectivity for CH_4 and NH_3, CN^- reduction of [FeCN] has high C_1 selectivity compared with other Fe catalysts. When considering the origin of this selectivity, it is worth noting that the addition of multiple cyanide ligands bound to Fe has not been observed during catalysis or chemical experiments. This might be critical for the high selectivity for the C_1 products. The precedent for C−C coupling of CO or CNR ligands at mononuclear metal sites requires two of these ligands bound to the metal prior to coupling.[64−67] The sterically encumbered, four-coordinate P_3^{Si} ligand hinders the facile addition of multiple equivalents of CN^-, maintaining the trigonal bipyramidal geometry during catalysis.[68] We propose that this results in high yields for C_1 products. Accordingly, the more flexible $(P_3^B)Fe$ platform[14,55] and the less encumbered $(PhBP^{iPr}_3)Fe$ platform[62] both have high C_2/C_1 ratios (0.16 and 0.11, respectively) compared to [FeCN] (0.02). Relatedly, a previously synthesized and stable compound, $(PhBP^{iPr}_3)Fe(CNR)_2$, demonstrates that $(PhBP^{iPr}_3)Fe$ could accommodate two CN^- ligands (or further protonated derivatives) in a 5-coordinate structure, likely needed for C_2 product formation.[69]

Finally, it is interesting to compare the strength of the reductant used herein for the CN^- reduction ($(C_6H_6)_2Cr$; $E°$ = −1.2 V), with a common reductant used for N_2R via related iron catalysts Cp^*_2Co ($E°$ = −1.9 V). Proposed pathways for catalysis require a turnover limiting potential ($E° \approx -2.0$ V) that generates an FeN_2^- species before protonation (to generate FeN_2H) can occur, necessitating reductants as strong as Cp^*_2Co.[38,40,70]

By contrast, the basicity of the CN^- ligand enables protonation of [FeCN] prior to an ET step.[25,36] Consequently, the turnover limiting potential is that of $[FeCNH]^{+/0}$ ($E°$ = −1.3 V), not $[FeCN]^{0/-}$ ($E°$= −2.1 V), allowing the use of a comparatively mild reductant like $(C_6H_6)_2Cr$. If initial protonation, or PCET, occurs before any independent ET steps, the turnover limiting potential for catalysis can be significantly less reducing. Indeed, Schrock's original triamidoamine Mo−N_2 catalyst system is thought to proceed via an initial PT step, and it is compatible with correspondingly milder reductants (e.g., Cp^*_2Cr) for turnover.[15,71,72]

CONCLUSIONS

In conclusion, we have described the catalytic reductive protonation of CN^- to primarily NH_3 and CH_4, by a mononuclear Fe complex, with selectivities comparable to those observed for CN^- reduction by nitrogenase. We also report mechanistic studies that show terminal iron aminocarbyne ($FeCNH_2$) intermediates, which are structurally similar to iron hydrazido intermediates ($FeNNH_2$) of Fe-mediated N_2R, as on-path in the CN^- reduction cycle. Experimental and computational studies suggest that these aminocarbynes undergo further C−H bond formation(s) prior to C−N bond cleavage, resulting in the selectivity observed, in contrast to iron hydrazidos during N_2R. Via this study, a terminal transition metal carbyne is hence invoked as a critical intermediate in the catalytic reductive protonation of a robust small molecule (CN^-).

ASSOCIATED CONTENT

Supporting Information

The Supporting Information is available free of charge at https://pubs.acs.org/doi/10.1021/jacs.3c12395.

Computational models (TXT)

Experimental methods; ammonia production and quantification studies; detection and quantification of gaseous products; additional control experiments; additional NMR experiments; ^{57}Fe Mössbauer spectroscopy; UV−vis spectroscopy; electrochemical methods; generation of proposed $[FeC(H)NMe_2]^+$; derivation of estimated BDFE (bond dissociation free energy) for early N−H bonds; and computational methods (PDF)

https://doi.org/10.1021/jacs.3c12395
J. Am. Chem. Soc. 2024, 146, 5343−5354

AUTHOR INFORMATION

Corresponding Author

Jonas C. Peters − *Division of Chemistry and Chemical Engineering, California Institute of Technology, Pasadena, California 91125, United States;* orcid.org/0000-0002-6610-4414; Email: jpeters@caltech.edu

Author

Christian M. Johansen − *Division of Chemistry and Chemical Engineering, California Institute of Technology, Pasadena, California 91125, United States;* orcid.org/0000-0003-0066-4424

Complete contact information is available at: https://pubs.acs.org/10.1021/jacs.3c12395

Author Contributions

The manuscript was written through contributions of all authors. All authors have given approval to the final version of the manuscript.

Funding

This study was funded by the National Institutes of Health (R01 GM-075757).

Notes

The authors declare no competing financial interest.

ACKNOWLEDGMENTS

We acknowledge support from NIH (GM-075757). We thank the Dow Next Generation Educator Fund and Instrumentation Grants for their support of the NMR facility at Caltech. We also thank the Resnick Sustainability Institute at Caltech for support of enabling facilities and instrumentation, including the RSI Water and Environment Lab (WEL). This research used resources of the National Energy Research Scientific Computing Center, a DOE Office of Science User Facility supported by the Office of Science of the U.S. Department of Energy under Contract No. DE-AC02-05CH11231 using NERSC award NERSC DDR-ERCAP0026667. C.M.J. is grateful for support from the Aker Scholarship foundation. We thank Dr. Nathan Dalleska and Dr. Nicholas Watkins for assistance with GC experiments and Dr. Sayan Bannerjee for assistance with computational studies.

ABBREVIATIONS

[TBA], tetrabutylammonium; OTf, triflate; BAr^F_4, tetrakis(3,5-bis(trifluoromethyl)phenyl)borate; Cp, cyclopentadienyl; Cp*, pentamethylcyclopentadienyl; (12-c-4), 12-crown-4 (1,4,7,10-tetraoxacyclododecane)

REFERENCES

(1) Seefeldt, L. C.; Yang, Z.-Y.; Lukoyanov, D. A.; Harris, D. F.; Dean, D. R.; Raugei, S.; Hoffman, B. M. Reduction of Substrates by Nitrogenases. *Chem. Rev.* **2020**, *120* (12), 5082−5106.

(2) Seefeldt, L. C.; Rasche, M. E.; Ensign, S. A. Carbonyl Sulfide and Carbon Dioxide as New Substrates, and Carbon Disulfide as a New Inhibitor, of Nitrogenase. *Biochemistry* **1995**, *34* (16), 5382−5389.

(3) Lee, C. C.; Hu, Y.; Ribbe, M. W. Vanadium Nitrogenase Reduces CO. *Science* **2010**, *329* (5992), 642−642.

(4) Spatzal, T.; Perez, K. A.; Einsle, O.; Howard, J. B.; Rees, D. C. Ligand Binding to the FeMo-Cofactor: Structures of CO-Bound and Reactivated Nitrogenase. *Science* **2014**, *345* (6204), 1620−1623.

(5) Hardy, R. W. F.; Knight, E. ATP-Dependent Reduction of Azide and HCN by N_2-Fixing Enzymes of Azotobacter Vinelandii and Clostridium Pasteurianum. *Biochim. Biophys. Acta BBA - Enzymol.* **1967**, *139* (1), 69−90.

(6) Kelly, M.; Postgate, J. R.; Richards, R. L. Reduction of Cyanide and isocyanide by Nitrogenase of Azotobacter Chroococcum. *Biochem. J.* **1967**, *102* (1), 1−3C.

(7) Li, J.; Burgess, B. K.; Corbin, J. L. Nitrogenase Reactivity: Cyanide as Substrate and Inhibitor. *Biochemistry* **1982**, *21* (18), 4393−4402.

(8) Lowe, D. J.; Fisher, K.; Thorneley, R. N. F.; Vaughn, S. A.; Burgess, B. K. Kinetics and Mechanism of the Reaction of Cyanide with Molybdenum Nitrogenase from Azotobacter Vinelandii. *Biochemistry* **1989**, *28* (21), 8460−8466.

(9) Fisher, K.; Dilworth, M. J.; Newton, W. E. Azotobacter Vinelandii Vanadium Nitrogenase: Formaldehyde Is a Product of Catalyzed HCN Reduction and Excess Ammonia Arises Directly from Catalyzed Azide Reduction. *Biochemistry* **2006**, *45* (13), 4190−4198.

(10) Lee, C. C.; Hu, Y.; Ribbe, M. W. ATP-Independent Hydrocarbon Formation Catalyzed by Isolated Nitrogenase Cofactors. *Angew. Chem., Int. Ed. Engl.* **2012**, *51* (8), 1947−1949.

(11) Lee, C. C.; Hu, Y.; Ribbe, M. W. Catalytic Reduction of CN^-, CO, and CO_2 by Nitrogenase Cofactors in Lanthanide-Driven Reactions. *Angew. Chem., Int. Ed. Engl.* **2015**, *54* (4), 1219−1222.

(12) Lee, C. C.; Hu, Y.; Ribbe, M. W. ATP-Independent Substrate Reduction by Nitrogenase P-Cluster Variant. *Proc. Natl. Acad. Sci. U. S. A.* **2012**, *109* (18), 6922−6926.

(13) Roth, L. E.; Tezcan, F. A. ATP-Uncoupled, Six-Electron Photoreduction of Hydrogen Cyanide to Methane by the Molybdenum−Iron Protein. *J. Am. Chem. Soc.* **2012**, *134* (20), 8416−8419.

(14) Chalkley, M. J.; Drover, M. W.; Peters, J. C. Catalytic N_2-to-NH_3 (or -N_2H_4) Conversion by Well-Defined Molecular Coordination Complexes. *Chem. Rev.* **2020**, *120* (12), 5582−5636.

(15) Yandulov, D. V.; Schrock, R. R. Catalytic Reduction of Dinitrogen to Ammonia at a Single Molybdenum Center. *Science* **2003**, *301* (5629), 76−78.

(16) Anderson, J. S.; Rittle, J.; Peters, J. C. Catalytic Conversion of Nitrogen to Ammonia by an Iron Model Complex. *Nature* **2013**, *501* (7465), 84−87.

(17) Hughes, D. L.; Mohammed, M. Y.; Pickett, C. J. Electroreduction of Co-Ordinated Cyanide to the Aminocarbyne Ligand (CNH_2) and a Pathway for Isomerisation of Ligating Methyleneamide (NCH_2): Reactions at Molybdenum of Relevance to Cyanide Reduction by Nitrogenase. *J. Chem. Soc. Chem. Commun.* **1989**, *18*, 1399−1400.

(18) Pombeiro, A. J. L.; Richards, R. L. Reactions of Alkynes, Isocyanides and Cyanides at Dinitrogen-Binding Transition Metal Centres. *Coord. Chem. Rev.* **1990**, *104* (1), 13−38.

(19) Pombeiro, A. J. L.; Guedes da Silva, M. F. C.; Michelin, R. A. Aminocarbyne Complexes Derived from Isocyanides Activated towards Electrophilic Addition. *Coord. Chem. Rev.* **2001**, *218*, 43−74.

(20) Tanifuji, K.; Sickerman, N.; Lee, C. C.; Nagasawa, T.; Miyazaki, K.; Ohki, Y.; Tatsumi, K.; Hu, Y.; Ribbe, M. W. Structure and Reactivity of an Asymmetric Synthetic Mimic of Nitrogenase Cofactor. *Angew. Chem., Int. Ed.* **2016**, *55* (50), 15633−15636.

(21) Sickerman, N. S.; Tanifuji, K.; Lee, C. C.; Ohki, Y.; Tatsumi, K.; Ribbe, M. W.; Hu, Y. Reduction of C_1 Substrates to Hydrocarbons by the Homometallic Precursor and Synthetic Mimic of the Nitrogenase Cofactor. *J. Am. Chem. Soc.* **2017**, *139* (2), 603−606.

(22) Tanifuji, K.; Lee, C. C.; Ohki, Y.; Tatsumi, K.; Hu, Y. L.; Ribbe, M. W. Combining a Nitrogenase Scaffold and a Synthetic Compound into an Artificial Enzyme. *Angew. Chem.-Int. Ed.* **2015**, *54* (47), 14022−14025.

(23) Fischer, E. O.; Schneider, J.; Neugebauer, D. $[(CO)_3PPh_3FeCN^iPr_2]^{\oplus}$, a Novel Stable Carbyneiron Complex Cation. *Angew. Chem., Int. Ed. Engl.* **1984**, *23* (10), 820−821.

(24) Mokhtarzadeh, C. C.; Moore, C. E.; Rheingold, A. L.; Figueroa, J. S. Terminal Iron carbyne Complexes Derived from Arrested CO_2 Reductive Disproportionation. *Angew. Chem., Int. Ed.* **2017**, *56* (36), 10894−10899.

(25) Rittle, J.; Peters, J. C. Proton-Coupled Reduction of an Iron Cyanide Complex to Methane and Ammonia. *Angew. Chem.-Int. Ed.* **2016**, *55* (40), 12262−12265.
(26) Lee, Y.; Peters, J. C. Silylation of Iron-Bound Carbon Monoxide Affords a Terminal Fe carbyne. *J. Am. Chem. Soc.* **2011**, *133* (12), 4438−4446.
(27) Anderson, J. S.; Cutsail, G. E.; Rittle, J.; Connor, B. A.; Gunderson, W. A.; Zhang, L.; Hoffman, B. M.; Peters, J. C. Characterization of an Fe≡N−NH_2 Intermediate Relevant to Catalytic N_2 Reduction to NH_3. *J. Am. Chem. Soc.* **2015**, *137* (24), 7803−7809.
(28) Rittle, J.; Peters, J. C. An Fe-N_2 Complex That Generates Hydrazine and Ammonia via Fe═NNH_2: Demonstrating a Hybrid Distal-to-Alternating Pathway for N_2 Reduction. *J. Am. Chem. Soc.* **2016**, *138* (12), 4243−4248.
(29) Thompson, N. B.; Green, M. T.; Peters, J. C. Nitrogen Fixation via a Terminal Fe(IV) Nitride. *J. Am. Chem. Soc.* **2017**, *139* (43), 15312−15315.
(30) Pombeiro, A. J. L.; Richards, R. L. Reactions of *trans*-$[Mo(CNMe)_2(PMe_2Ph)_4]$ and *mer*-$[W(CNMe)_3(PMe_2Ph)_3]$ Complexes with Methanol and with Mineral Acids to Give Amines, Ammonia and Hydrocarbons. *Transit. Met. Chem.* **1980**, *5* (1), 281−284.
(31) Carvalho, M. F. N. N.; Pombeiro, A. J. L.; Schubert, U.; Orama, O.; Pickett, C. J.; Richards, R. L. Preparation and Properties of *Mer*-$[ReCl(N_2)(CNR)\{P(OMe)_3\}_3]$(R = Me, Et, Bu^t, $C_6H_4^{Me\text{-}4}$, or $C_6H_4^{Cl\text{-}4}$) and $[ReCl(N_2)(CNMe)(PPh_3)\{P(OEt)_3\}_2]$. X-Ray Crystal Structure of *Mer*-$[ReCl(N_2)(CNMe)\{P(OMe)_3\}_3]$ and Reductive Cleavage of the isocyanide Ligands to Primary Amines upon Protonation. *J. Chem. Soc. Dalton Trans.* **1985**, *10*, 2079−2084.
(32) For an example of protonation and substrate release from a bridging carbyne see: Whitmire, K.; Shriver, D. F. A New Reaction for the Conversion of Carbon Monoxide into Methane: Proton-Induced Reduction of Carbon Monoxide in a Metal Carbonyl Cluster, $[Fe_4(CO)_{13}^{2-}]$. *J. Am. Chem. Soc.* **1980**, *102* (4), 1456−1457.
(33) Holt, E. M.; Whitmire, K. H.; Shriver, D. F. The Role of Metal Cluster Interactions in the Proton-Induced Reduction of CO. the Crystal Structures of $[PPN]\{HFe_4(CO)_{12}\}$ and $HFe_4(CO)_{12}(\eta\text{-}COCH_3)$. *J. Organomet. Chem.* **1981**, *213* (1), 125−137.
(34) Wengrovius, J. H.; Sancho, J.; Schrock, R. R. Metathesis of Acetylenes by Tungsten(VI)-Alkylidyne Complexes. *J. Am. Chem. Soc.* **1981**, *103* (13), 3932−3934.
(35) Fürstner, A. The Ascent of Alkyne Metathesis to Strategy-Level Status. *J. Am. Chem. Soc.* **2021**, *143* (38), 15538−15555.
(36) Rittle, J.; Peters, J. C. N−H Bond Dissociation Enthalpies and Facile H Atom Transfers for Early Intermediates of Fe−N_2 and Fe−CN Reductions. *J. Am. Chem. Soc.* **2017**, *139* (8), 3161−3170.
(37) Chalkley, M. J.; Oyala, P. H.; Peters, J. C. Cp* Noninnocence Leads to a Remarkably Weak C−H Bond via Metallocene Protonation. *J. Am. Chem. Soc.* **2019**, *141* (11), 4721−4729.
(38) Chalkley, M. J.; Del Castillo, T. J.; Matson, B. D.; Peters, J. C. Fe-Mediated Nitrogen Fixation with a Metallocene Mediator: Exploring pK_a Effects and Demonstrating Electrocatalysis. *J. Am. Chem. Soc.* **2018**, *140* (19), 6122−6129.
(39) Connelly, N. G.; Geiger, W. E. Chemical Redox Agents for Organometallic Chemistry. *Chem. Rev.* **1996**, *96* (2), 877−910.
(40) Chalkley, M. J.; Del Castillo, T. J.; Matson, B. D.; Roddy, J. P.; Peters, J. C. Catalytic N_2-to-NH_3 Conversion by Fe at Lower Driving Force: A Proposed Role for Metallocene-Mediated PCET. *ACS Cent. Sci.* **2017**, *3* (3), 217−223.
(41) Ung, G.; Peters, J. C. Low-Temperature N_2 Binding to Two-Coordinate L_2Fe^0 Enables Reductive Trapping of $L_2FeN_2^-$ and NH_3 Generation. *Angew. Chem., Int. Ed.* **2015**, *54* (2), 532−535.
(42) Betley, T. A.; Peters, J. C. Dinitrogen Chemistry from Trigonally Coordinated Iron and Cobalt Platforms. *J. Am. Chem. Soc.* **2003**, *125* (36), 10782−10783.
(43) Del Castillo, T. J.; Thompson, N. B.; Peters, J. C. A Synthetic Single-Site Fe Nitrogenase: High Turnover, Freeze-Quench ^{57}Fe Mössbauer Data, and a Hydride Resting State. *J. Am. Chem. Soc.* **2016**, *138* (16), 5341−5350.
(44) Citek, C.; Oyala, P. H.; Peters, J. C. Mononuclear Fe(I) and Fe(II) Acetylene Adducts and Their Reductive Protonation to Terminal Fe(IV) and Fe(V) carbynes. *J. Am. Chem. Soc.* **2019**, *141* (38), 15211−15221.
(45) Buscagan, T. M.; Oyala, P. H.; Peters, J. C. N_2-to-NH_3 Conversion by a Triphos−Iron Catalyst and Enhanced Turnover under Photolysis. *Angew. Chem., Int. Ed.* **2017**, *56* (24), 6921−6926.
(46) Creutz, S. E.; Peters, J. C. Exploring Secondary-Sphere Interactions in Fe−N_xH_y Complexes Relevant to N_2 Fixation. *Chem. Sci.* **2017**, *8* (3), 2321−2328.
(47) The protonation of [FeCN] to $[FeCNH][BAr^F{}_4]$ was monitored by observing the shift in the UV−visible spectra maxima at 910 and 540 nm to 790 and 610 nm upon addition of the acid, see SI.
(48) Addition of more equivalents $(C_6H_6)_2Cr$ was not possible due to solubility limitations interfering with the UV−vis measurements.
(49) Garrido-Barros, P.; Chalkley, M. J.; Peters, J. C. Light Alters the NH_3 vs N_2H_4 Product Profile in Iron-Catalyzed Nitrogen Reduction via Dual Reactivity from an Iron hydrazido (Fe═NNH_2) Intermediate. *Angew. Chem., Int. Ed.* **2023**, *62* (9), No. e202216693.
(50) Boyd, E. A.; Peters, J. C. Highly Selective Fe-Catalyzed Nitrogen Fixation to Hydrazine Enabled by Sm(II) Reagents with Tailored Redox Potential and pK_a. *J. Am. Chem. Soc.* **2023**, *145* (27), 14784−14792.
(51) The observation of substantial amounts of Me_3N is perhaps unexpected given the selectivity for NH_3 + CH_4 in the catalytic cyanide reduction reaction. We note that while $[FeCNMe_2]$ and $[FeCNH_2]^{+/0}$ react with a combination of $(C_6H_6)_2Cr/Ph_2NH_2]OTf$ at similar rates, the proposed intermediate $[FeC(H)NMe_2]^+$ is consumed much more slowly. This could suggest an alternative reaction pathway, such as bimolecular Me• transfer.
(52) L represents a 2 e^- ligand (e.g., carbene, CO, CNMe, N_2). Relevant Mössbauer data for other S = 1 species, where $(P_3^{Si})Fe^{II}$−L^+ represents the cationic species $(P_3^{Si})Fe(CO)^+$, $(P_3^{Si})Fe(CNMe)^+$, and $(P_3^{Si})Fe(N_2)^+$, are: δ = 0.31 mm s^{-1}, ΔE_Q = 4.12 mm s^{-1} ; δ = 0.41 mm s^{-1}, ΔE_Q = 3.14 mm s^{-1}; δ = 0.53 mm s^{-1}, ΔE_Q = 2.39 mm s^{-1} respectively.
(53) Tao, J.; Perdew, J. P.; Staroverov, V. N.; Scuseria, G. E. Climbing the Density Functional Ladder: Nonempirical Meta-Generalized Gradient Approximation Designed for Molecules and Solids. *Phys. Rev. Lett.* **2003**, *91* (14), 146401−146404.
(54) Weigend, F. Accurate Coulomb-Fitting Basis Sets for H to Rn. *Phys. Chem. Chem. Phys.* **2006**, *8* (9), 1057−1065.
(55) Matson, B. D.; Peters, J. C. Fe-Mediated HER vs N_2RR: Exploring Factors That Contribute to Selectivity in $P_3^EFe(N_2)$ (E = B, Si, C) Catalyst Model Systems. *ACS Catal.* **2018**, *8* (2), 1448−1455.
(56) As an example, explicit solvent interactions are often required to accurately predict reduction potentials, as recently observed for persulfate oxidation: Hosseini, S.; Janusz, J. N.; Tanwar, M.; Pendergast, A. D.; Neurock, M.; White, H. S. Oxidation by Reduction: Efficient and Selective Oxidation of Alcohols by the Electrocatalytic Reduction of Peroxydisulfate. *J. Am. Chem. Soc.* **2022**, *144* (46), 21103−21115.
(57) Jolly, P. W.; Pettit, R. Evidence for a Novel Metal-Carbene System. *J. Am. Chem. Soc.* **1966**, *88* (21), 5044−5045.
(58) Brookhart, M.; Tucker, J. R.; Flood, T. C.; Jensen, J. Spectroscopic Characterization of an Electrophilic Transition-Metal-Methylene Complex, η^5-$C_5H_5[(C_6H_5)_2PCH_2CH_2P(C_6H_5)_2]Fe{:}CH_2^+$. *J. Am. Chem. Soc.* **1980**, *102* (3), 1203−1205.
(59) Aghazada, S.; Munz, D.; Heinemann, F. W.; Scheurer, A.; Meyer, K. A Crystalline Iron Terminal methylidene. *J. Am. Chem. Soc.* **2021**, *143* (41), 17219−17225.
(60) Lee, Y.; Mankad, N. P.; Peters, J. C. Triggering N_2 Uptake via Redox-Induced Expulsion of Coordinated NH_3 and N_2 Silylation at Trigonal bipyramidal Iron. *Nat. Chem.* **2010**, *2* (7), 558−565.
(61) Benson, S. W. III - Bond Energies. *J. Chem. Educ.* **1965**, *42* (9), 502.

https://doi.org/10.1021/jacs.3c12395
J. Am. Chem. Soc. 2024, 146, 5343−5354

(62) Mankad, N. P.; Whited, M. T.; Peters, J. C. Terminal $Fe^{I}-N_2$ and $Fe^{II}\cdots H-C$ Interactions Supported by Tris(phosphino)Silyl Ligands. *Angew. Chem., Int. Ed.* **2007**, *46*, 5768−5771.
(63) Attempts to optimize $[Fe{=}C(H)NH_3]^0$ showed *in silico* C−N bond cleavage; the energy of this intermediate was hence estimated by constrained geometry optimization with the C−N bond set to 1.6 Å.
(64) Suess, D. L. M.; Peters, J. C. A CO-Derived Iron Dicarbyne That Releases Olefin upon Hydrogenation. *J. Am. Chem. Soc.* **2013**, *135* (34), 12580−12583.
(65) Wang, Y.; Da Silva, J. J. R. F.; Pombeiro, A. J. L.; Pellinghelli, M. A.; Tiripicchio, A.; Henderson, R. A.; Richards, R. L. Aminocarbyne Coupling Reactions at $M(Ph_2PCH_2CH_2PPh_2)_2$ (M = Mo or W) Sites. Synthesis and Properties of the Diaminoacetylene Complexes *trans*-$[MX(\eta^2\text{-}MeHNC{\equiv}CNHMe)\text{-}(Ph_2PCH_2CH_2PPh_2)_2]A$ (X = F, Cl or ClO_4; A = BF_4, PF_6, HCl_2 or ClO_4) and of Their Di(Aminocarbyne)-Type Precursors. *J. Chem. Soc., Dalton Trans.* **1995**, No. 7, 1183−1191.
(66) Filippou, A. C.; Grünleitner, W.; Völkl, C.; Kiprof, P. Metal-Centered Coupling of Two carbyne Ligands To Form an Alkyne Ligand. *Angew. Chem., Int. Ed. Engl.* **1991**, *30* (9), 1167−1169.
(67) Filippou, A. C.; Völkl, C.; Grünleitner, W.; Kiprof, P. carbyne-carbyne Coupling at a Single Metal Center. Synthesis Structure of Bis(Diethylamino)Acetylene Complexes of Molybdenum(II) and Tungsten(II). *J. Organomet. Chem.* **1992**, *434* (2), 201−223.
(68) The overaddition of CN^- ligand was not observed in the reaction of (P_3^{Si})FeOTf and [TBA][CN]. Similarly, (P_3^{Si})FeCN is synthesized with excess NaCN in refluxing 1:1 THF:MeOH, but addition of multiple equivalents of CN^- has not been observed.
(69) Turculet, L.; Feldman, J. D.; Tilley, T. D. Coordinatively and Electronically Unsaturated Zwitterionic Iron Silyl Complexes Featuring the Tripodal phosphine Ligand $[PhB(CH_2P^iPr_2)_3]^-$. *Organometallics* **2003**, *22* (23), 4627−4629.
(70) Hill, P. J.; Doyle, L. R.; Crawford, A. D.; Myers, W. K.; Ashley, A. E. Selective Catalytic Reduction of N_2 to N_2H_4 by a Simple Fe Complex. *J. Am. Chem. Soc.* **2016**, *138* (41), 13521−13524.
(71) Yandulov, D. V.; Schrock, R. R. Studies Relevant to Catalytic Reduction of Dinitrogen to Ammonia by Molybdenum Triamidoamine Complexes. *Inorg. Chem.* **2005**, *44* (4), 1103−1117.
(72) Thimm, W.; Gradert, C.; Broda, H.; Wennmohs, F.; Neese, F.; Tuczek, F. Free Reaction Enthalpy Profile of the Schrock Cycle Derived from Density Functional Theory Calculations on the Full $[MoHIPTN_3N]$. *Catalyst. Inorg. Chem.* **2015**, *54* (19), 9248−9255.

https://doi.org/10.1021/jacs.3c12395
J. Am. Chem. Soc. 2024, 146, 5343−5354